

We are IntechOpen, the world's leading publisher of Open Access books Built by scientists, for scientists

6,900

Open access books available

185,000

International authors and editors

200M

Downloads

Our authors are among the

154

Countries delivered to

TOP 1%

most cited scientists

12.2%

Contributors from top 500 universities



WEB OF SCIENCE™

Selection of our books indexed in the Book Citation Index
in Web of Science™ Core Collection (BKCI)

Interested in publishing with us?
Contact book.department@intechopen.com

Numbers displayed above are based on latest data collected.
For more information visit www.intechopen.com



Multiple Andreev Reflections and Enhanced Quantum Interferences with Reentrant Behavior in NbN/Network-like Carbon Nanotubes/NbN SNS Junctions

Yuan-Liang Zhong¹, Hayato Nakano², Tatsushi Akazaki³
and Hideaki Takayanagi⁴

¹*Department of Physics, Chung Yuan Christian University*

^{2,3}*NTT Basic Research Laboratories, NTT Corporation*

⁴*Department of Applied Physics, Tokyo University of Science*

¹*Taiwan*

^{2,3,4}*Japan*

1. Introduction

The superconducting proximity effect has been studied in superconductor (S)/normal conductor (N) junctions or SNS junctions for a few decades. If a clean contact is brought into an SN junction, some Cooper pairs will penetrate into the normal conductor from the superconductor to form an incident electron and a retroreflected hole in it. This process is called Andreev reflection (AR). If both electrodes are superconducting, two SN junctions with very-low-barrier tunnel junctions, a series of ARs can be observed in the differential resistance at submultiples of gap voltage, $2\Delta/ne$, where $n=1,2,\dots$ (Octavio et al., 1983) and Δ is superconducting energy gap. These subharmonic gap structures (SGS) occurring at the maximum slopes of differential resistance are due to multiple Andreev reflection (MAR) (Bezuglyi et al., 2000). If the ARs can be bounded at the two SN boundaries to confine the electron-hole motion spatially in the normal region, these Andreev bound states are localized states carrying finite supercurrent. The AR process has been studied in ballistic and diffusive SNS junctions using metal, the two-dimensional electron gas (2DEG) of semiconductor heterostructures (Hoss et al., 2000; Nitta et al., 1994; Octavio et al., 1983), carbon nanotubes (Bezuglyi et al., 2000) and graphene (Dirks et al., 2011) as normal conductor. Carbon nanotubes (CNTs) with a diameter of only a few nm as normal conductors are one of the best candidates for studying quasi one-dimensional (1D) proximity effect and AR. Though some experiments and theories have demonstrated 1D Tomonaga-Luttinger liquid behavior in single-wall carbon nanotube (SWNT) or even multi-wall CNT (MWNT) (Bockrath et al., 1999), some experiments have shown AR (Morpurgo et al., 1999), MAR (Jarillo-Herrero et al., 2006; Buitelaar et al., 2003; Jorgensen et al., 2006), Andreev bound states (Pillet et al., 2010) and supercurrent in CNTs (Jarillo-Herrero et al., 2006; Kasumov et al., 1999),

and even superconducting quantum interference device made with CNTs (Cleuziou et al., 2006).

The superconducting proximity effect in the network-like structure with quasi-1D CNT will be discussed in the chapter. The enhanced quantum interferences can be given rise to as Aharonov-Bohm (AB)-type oscillations due to the loops as AB ring in the network-like structure by applied magnetic field. We have studied the MAR and enhanced quantum interferences, and the reentrant behavior of conductance in this random network CNT.

The updated superconducting proximity effect theory for reentrant behavior has shown that the proximity correction to the conductance $\Delta G_N(V, T, B)$ disappears at low energies and reaches a maximum value around temperature T or bias voltage V corresponding to the Thouless energy (correlation energy), E_{th} constant (Volkov & Takayanagi, 1997; Golubov, Wilhelm & Zaikin, 1997; Nakano & Takayanagi, 2000) (see Fig. 12). This reentrant behavior in ΔG_N occurs near $eV \cong E_{th}$, $k_B T \cong E_{th}$, or $B \cong B_c$, where B_c is a correlation magnetic field. The reentrant behavior has also been predicted for magnetoconductance oscillations, but has not been completely observed in experiment yet. In what follows, we also present the MAR in magnetic field and then demonstrate the reentrant behavior of the conductance and magnetoconductance fluctuations.

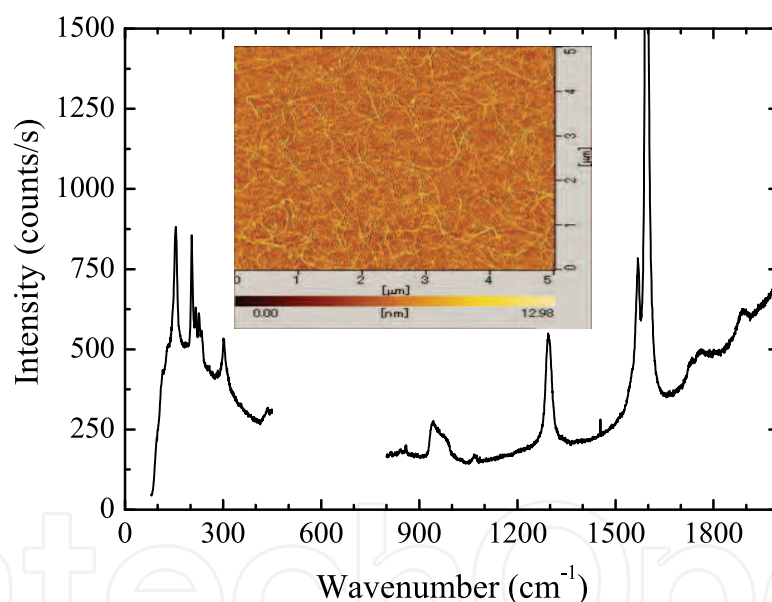


Fig. 1. Raman spectra of carbon nanotubes taken with 785-nm excitation from a sample consisting CNTs on SiO_2/Si substrate. The Raman spectra peaks of carbon nanotubes, RBM modes at $\sim 200 \text{ cm}^{-1}$, the high-energy graphitelike mode at $\sim 1600 \text{ cm}^{-1}$ and the defect-induced D mode at $\sim 1300 \text{ cm}^{-1}$, were observed. Inset: Carbon nanotubes on SiO_2/Si wafer substrate.

2. Fabrication of carbon nanotubes bridging superconducting electrodes

2.1 Fabrication of carbon nanotubes

CNTs were synthesized on a silicon wafer with 100-nm-thick thermal oxide by the chemical vapor deposition method using Co catalyst. A Co film is about 0.1-0.3 nm thick by

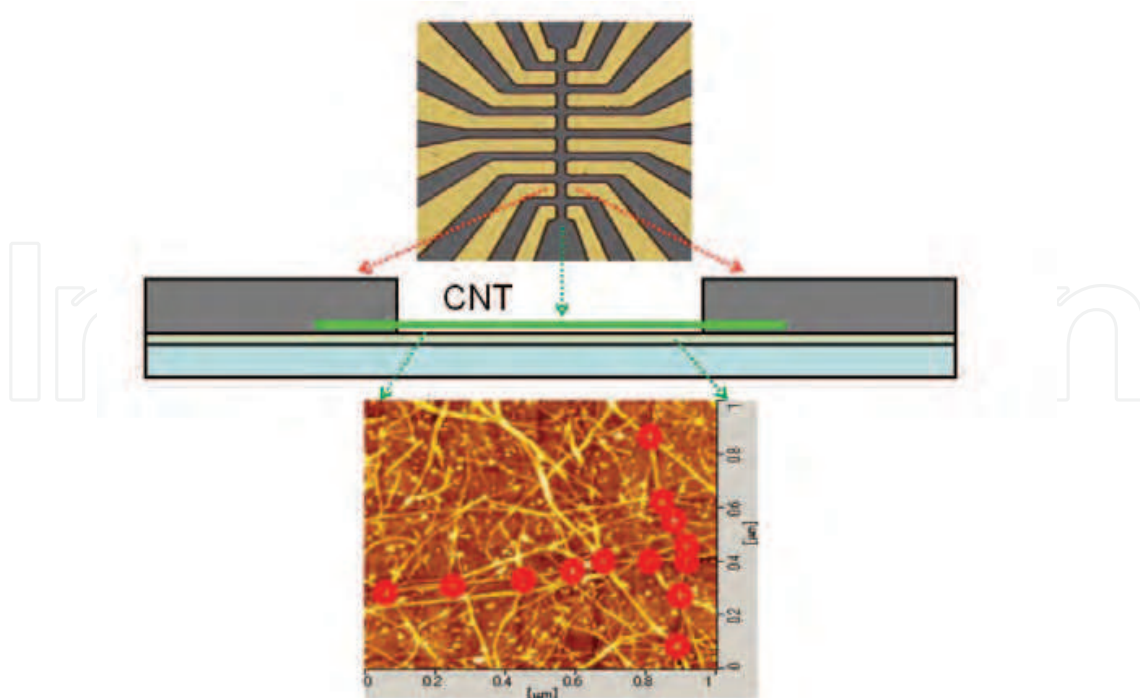


Fig. 2. Schematics of NbN/Network-like Carbon Nanotubes/NbN SNS Junctions (middle). The patterns of NbN electrodes (top) and an AFM image of the CNTs device (bottom) are made on SiO_2 substrate. The circle marks indicate the crossed junction of carbon nanotubes (bottom)

electron-beam deposition. The diameter of the Co nanoparticles control the diameter of the CNTs. For the synthesis procedure, argon gas fed into the furnace was heated to reach the growth temperature of $900\text{-}1000^\circ\text{C}$ and then replaced by pure methane at a flow rate $300\text{ cm}^3/\text{min}$ with the pressure of 500 Torr for 5-10 min. This growth condition is optimized for SWNT growth and we observed very few MWNTs in TEM and AFM images. Inset of Fig. 1 shows the carbon nanotubes on the SiO_2 substrate. The CNTs belong to the SWNTs of individual nanotubes or bundles, which were measured from the height of each nanotube in an AFM (the CNTs with the diameter of 1-3 nm) and was confirmed by Raman spectra measurement. Raman spectroscopy technique was used to measure the characteristic of carbon nanotubes to show in Fig. 1. The diameter-selective Raman scattering is particularly important for the Raman band at about 200 cm^{-1} , which is associated with the radical breathing mode (RBM) of the carbon nanotube (Rao et al.,1997), to indicate the characteristic of SWNTs and sharp high energy graphite-like mode (G band) are also supported this results. The CNTs were freely synthesized to form random network structures, as shown in the inset of Fig. 1.

2.2 Fabrication of superconducting electrodes

The CNTs are growth between the electrodes with Co catalyst patterns using lithography technique. The CNTs were directly connected to NbN electrodes as shown in Fig. 2. Between the electrodes were designed to be $1.5\text{ }\mu\text{m}$ length on the photomask. The number of CNTs between the NbN electrodes was roughly estimated to be about 1000-2000. These network-like CNTs have the characteristic of quasi-diffusive transport, which is due to the network structure including defects, bundles and crossed junctions that marked in the bottom

figure of Fig. 2. A excellent superconducting properties for NbN electrodes with 100-nm thickness and 1- μm wide have typically high superconducting critical temperature $T_c \sim 15$ K and high superconducting critical magnetic field $H_{c2} \gtrsim 20$ T. Optimum ohmic contact in junctions was made by annealing. The samples in vacuum were annealed with an infrared heater at 700°C for ~ 15 min and contact resistance was reduced nearly 1~2 orders of magnitude. After the annealing, the T_c of NbN electrodes is close to 11 K. The samples were measured using the lock-in technique and four-probe method in a helium cryostat.

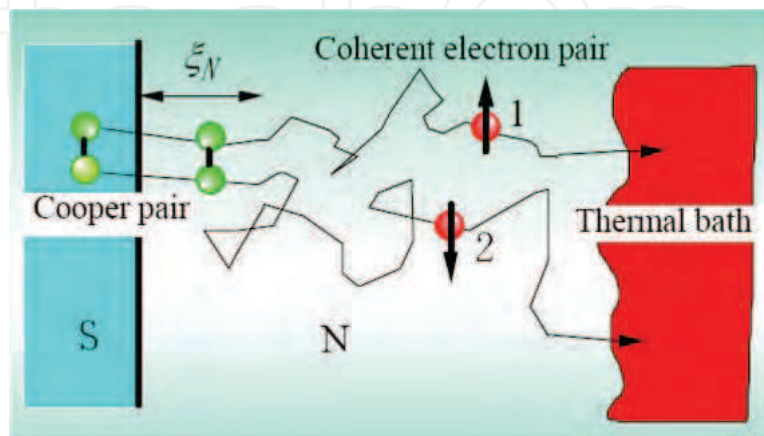


Fig. 3. The schematic process of Cooper pairs into normal conductor given rise by superconducting proximity effect

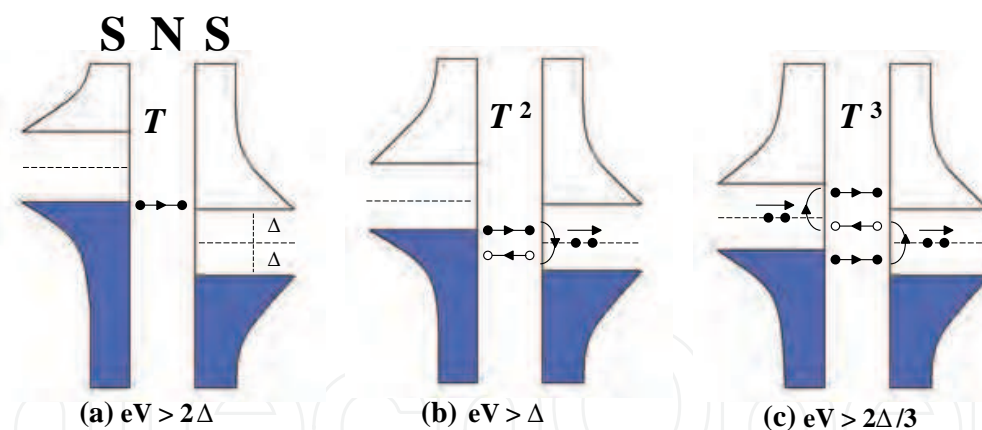


Fig. 4. Schematic process of (a) normal transport, (b) AR, and (c) MAR. There are different electron transparent probability T shown on figure for different transport processes

3. Superconducting proximity effect and Andreev reflection

The Cooper pairs into normal conductor diffusive process is given rise by superconducting proximity effect shown in Fig 3. In the junction of SN-thermal bath, Cooper pairs into normal diffusive conductor move within a distance called thermal coherent length, $\xi_T = \sqrt{\hbar D / 2\pi k_B T}$, before breaking, and then keep coherence in the phase of two electron called coherent electron pairs. Cooper pairs leak into normal-conductor side from superconductor as

generating correlated electron-hole pairs at SN interference called Andreev reflection. Figure 4 shows a processes of AR. For electron voltage higher than superconducting energy gap Δ (see Fig. 4(a)), electron merely transport in normal process. For electron voltage lower than Δ (see Fig. 4(b)(c)), Cooper pairs leak at SN junction to create Andreev reflection (Fig. 4(b)) and even MAR (Fig. 4(c)).

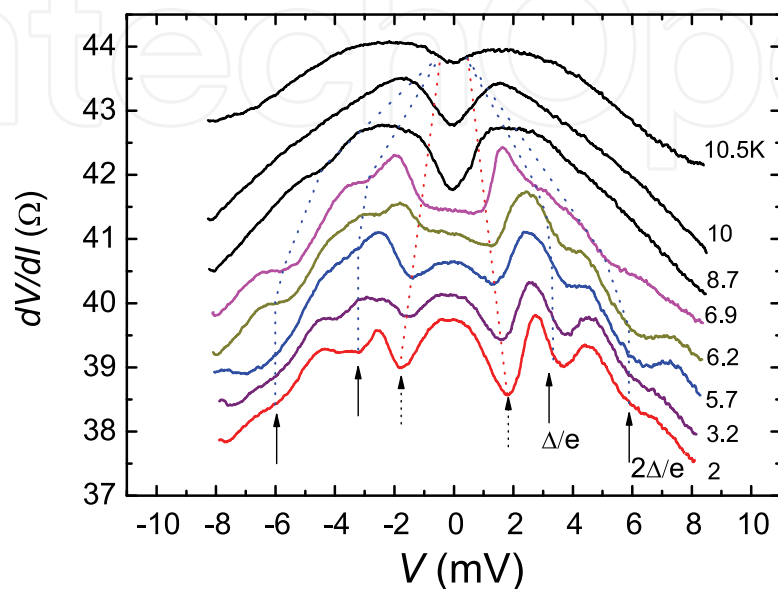


Fig. 5. Differential resistance as a function of applied voltage at different constant temperature between 2 and 11 K. The resistances are offset from each other for clarity. MAR occurs at 3 and 6 meV (solid line arrows) and AR occurs at zero-bias voltage above around 9 K.

The MAR was observed by measuring differential resistance as a function of applied voltage. Figure 5 shows SGS due to the MAR (Bezuglyi et. al.,2000; Hoss et. al.,2000; Nitta et al.,1994) and the submultiples of the gap voltage, $\pm 2\Delta/e$ and $\pm \Delta/e$ (solid line arrows). The MAR become smeared gradually at temperature above ~ 7 K and then a dip of the AR is observed at more high temperature but below T_c , 11 K. In addition, the MAR and AR were observed in different constant magnetic field between 0 and 4.3 T at temperature 1.75 K (Fig. 6). The SGS and AR dip become smeared above ~ 450 mT and ~ 1.5 T, respectively. Previous experiments on 2D SNS junctions based on clean semiconductor heterostructures have also observed the MAR and AR smeared in the magnetic field (Nitta et al.,1994), but only below a few μ T. The suppression of MAR and AR in a magnetic field can be easily understood by a physical process shown in Fig. 7. The AR takes place at the SN interfaces, and quasi-particles trajectories are deflected and the angle of incidence is increased. Because the parallel momentum becomes larger than the perpendicular momentum, the AR probability is suppressed (Mortensen et al.,1999). Though the smearing mechanism is the same as other dimensions, owing to 1D CNTs with small diameters, the quasiparticles are not easily deflected and their parallel moment not easily enhanced during motion as schematic process. Therefore, the applied magnetic field for seaming AR is larger than other dimensions over two orders of magnitude.

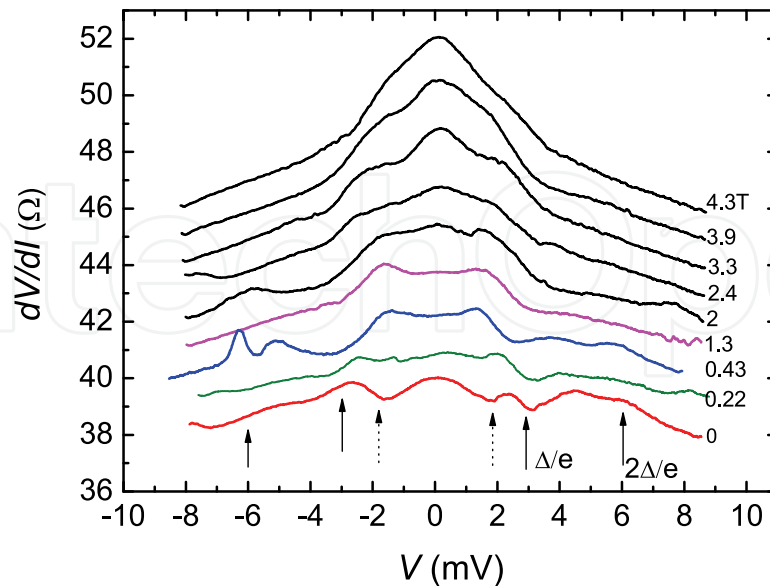


Fig. 6. Differential resistance as a function of applied voltage in constant magnetic field below 4.3 T. MAR processes occur at 3 and 6 meV (solid line arrows) and reentrant behavior occur at close zero zero bias (dash line arrows). The MAR is smeared by applying magnetic field over ~ 250 mT. Above 0.4 T, the curves of peak are changed to dip at around zero bias voltage. ARs disappear at over 2 T.

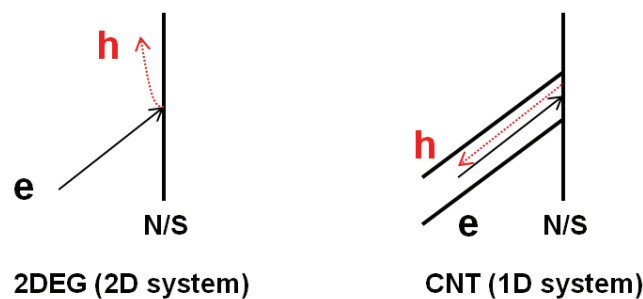


Fig. 7. Schematic process of the AR in 2DEG (2D system) and CNT (1D system) at NS junction with an incident electron (e) and a retroreflected hole (h) in an applied magnetic field below mT. The electron and hole can not be easily deflected in CNT compared with 2DEG in applied magnetic field and are still confined in CNT

4. Magnetoconductance fluctuations and enhanced quantum interference

A single electronic wave that is split into two propagating waves over different paths as shown in Fig. 8. The quantum interference of electron will be modulated by an applied magnetic field passed through in the ring. The oscillations in conductance due to this AR effect can be observed in the conductor ring of ballistic transport by measuring magnetoconductance. In the metallic wire within mesoscopic scale of diffusive transport, a single electron that scatters around the closed path and interference with itself by impurities scattering to cause AB effect in some loops. Some oscillations by loops in wire will be formed fluctuations in conductance called universal conductance fluctuations (UCF). Some loops in network-like CNT as the interference loops are shown in Fig. 9.

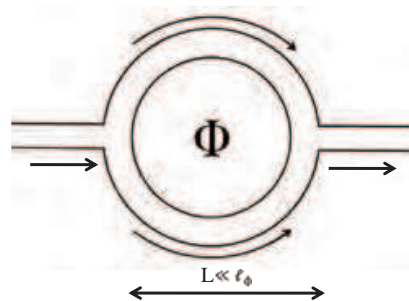


Fig. 8. AB ring with an applied magnetic field passed through caused quantum interferences from electronic wave splitting into two different paths

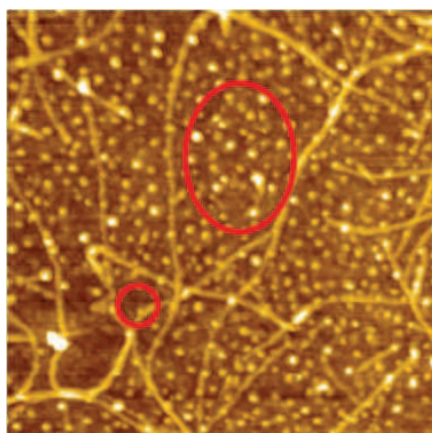


Fig. 9. Some loops in network-like CNTs as the AB rings

We have observed enhanced magnetoconductance fluctuations (EMF) by magnetoconductance measurement. The magnetoconductance fluctuations were measured by applying a magnetic field of up to 3 or 4 T at temperature between 10 and 4 K (Fig. 10). In the inset of Fig. 10, the two curves at 8 K (dash and solid curve) show reproducible fluctuations and those curves at temperatures 8, 9.2 and 9.6 K also show similar fluctuation structures. The fluctuation amplitudes become large from ~ 10 to 8 K (the inset of Fig. 10). The other similar fluctuation structures become small from 8 to 4 K as shown in Fig. 11. This reentrant behavior of magnetoconductance fluctuations will be discussed in more detail later. These fluctuations are similar to AB-type oscillation caused by the loops in a network-like structure. The AB-type interferences can be formed in the loops by applying magnetic field. Owing to the loops of different size, the magnetoconductance fluctuations look like the UCFs observed in metallic wire (Washburn&Webb,1992).

The fluctuation amplitude (ΔG_f) is larger than $\sim e^2/h$, the normal UCF amplitude. The enhanced magnetoconductance fluctuations can be as a superconducting UCFs. The larger amplitude indicates that the fluctuations are not due to normal quantum interference, but due to Andreev quasiparticle interference. From the evaluated number of loops, about 10^6 (about 10 crossed junctions between electrodes), we can obtain theoretically the maximum amplitude of $\sim 4e^2/h$ compared with the $\sim 6e^2/h$ in the inset of Fig. 10. (see the details in section 6).

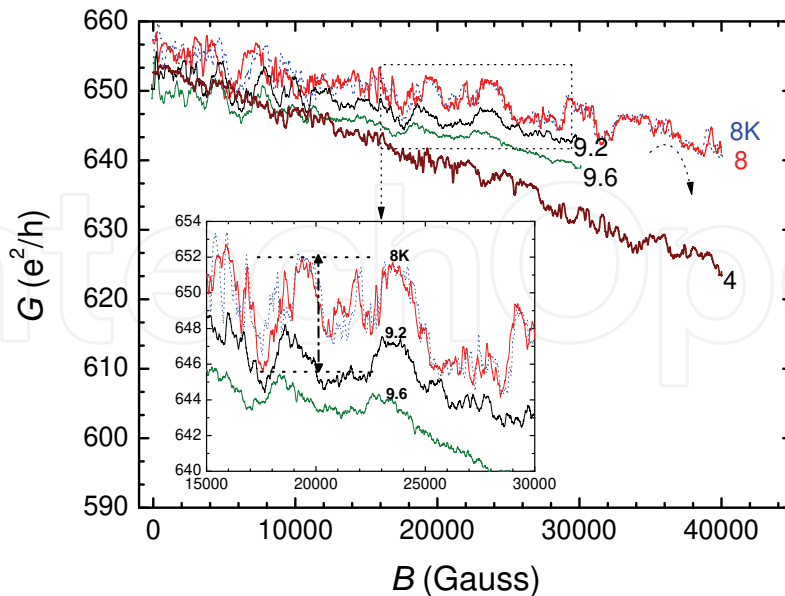


Fig. 10. EMF at different constant temperature between 10 and 4 K. The fluctuations have a maximum amplitude at around 8 K. Inset: reproducible fluctuations at 8 K (the dash and solid curve) and three similar curves of fluctuations at 8, 9.2 and 9.6 K.

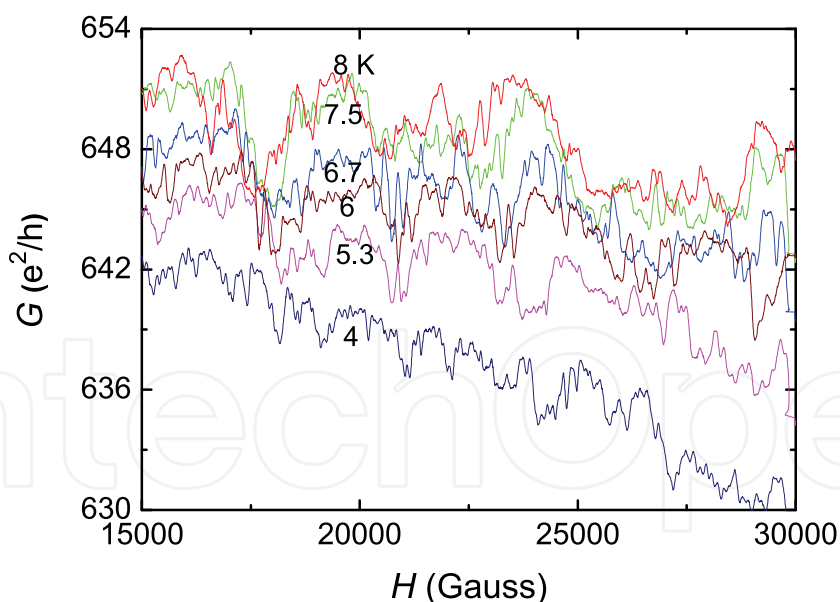


Fig. 11. EMF at the variation of temperatures. The similar curves of fluctuations are shown at 8, 7.5, 6.7, 6, 5.3 and 4 K

5. Reentrant behavior caused by superconducting proximity effect

For superconducting proximity effect in the conductor of diffusive transport, a updated superconducting proximity effect theory has shown that the proximity correction to the

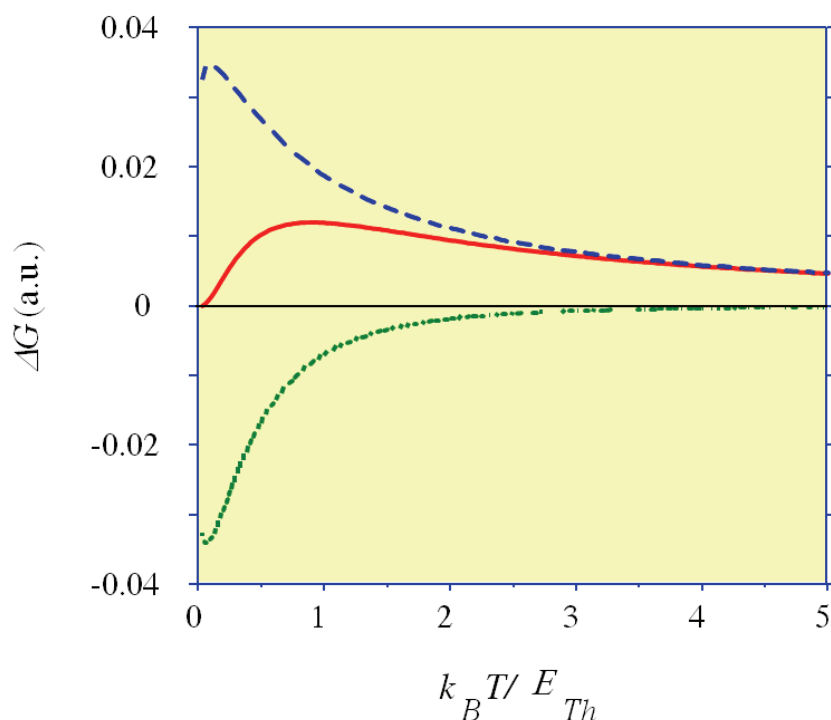


Fig. 12. The reentrant behavior of the red curve predicted by the updated superconducting proximity effect theory (solid curve). The blue curve from MTSF effect (long dash curve) and the green curve from DDOS effect (short dash curve), two effects contribute to reentrant behavior

conductance ($\Delta G_N(V, T, B)$) disappears at low energies and reaches a maximum value around temperature T or bias voltage V corresponding to the Thouless energy (correlation energy), $E_{th} \equiv \hbar D/L^2$, where D and L are the diffusion constant and sample length (Volkov&Takayanagi,1997; Golubov,Wilhelm&Zaikin,1997; Nakano&Takayanagi,2000), as shown in Fig. 12. Two effects, the Maki-Thompson-type of superconducting fluctuation(MTSF) effect and the decreased quasiparticles density of states (DDOS) effect at the Fermi level, contribute to $\Delta G_N(V, T, B)$. These two contributions become equal and cancel each other out exactly at the absolute zero-temperature or at the zero-bias voltage limit as shown in the middle curve (red curve) of Fig. 12. This reentrant behavior has also been predicted for the temperature dependance of magnetoconductance fluctuations $\Delta G_f(T)$ and the magnetic field dependance of magnetoconductance fluctuations $\Delta G_f(B)$.

The differential resistance near zero-bias voltage that has been observed a reentrant behavior. As shown in Fig. 5, the reentrant behavior was observed in the voltage dependance of differential resistance at 2 K. The differential resistance becomes larger as the applied voltage approaches zero voltage and reaches a minimum value (dip), ~ 1.8 mV (dash line arrows), near zero-bias. This dip is due to the reentrant effect on voltage and is similar to E_{th} . The differential resistance of zero-bias voltage from the peak to dip varies with temperature between 2 and 11 K (Fig. 5), which is transformed into the conductance as a function of temperature as shown in the inset of Fig.13. The conductance becomes higher and reaches a maximum at about 8 K related to E_{th} , and then becomes lower at low temperature. This reentrant behavior of conductance have been studied in both theory (Golubov,Wilhelm&Zaikin,1997; Volkov&Takayanagi,1997; Nakano&Takayanagi,2000) and

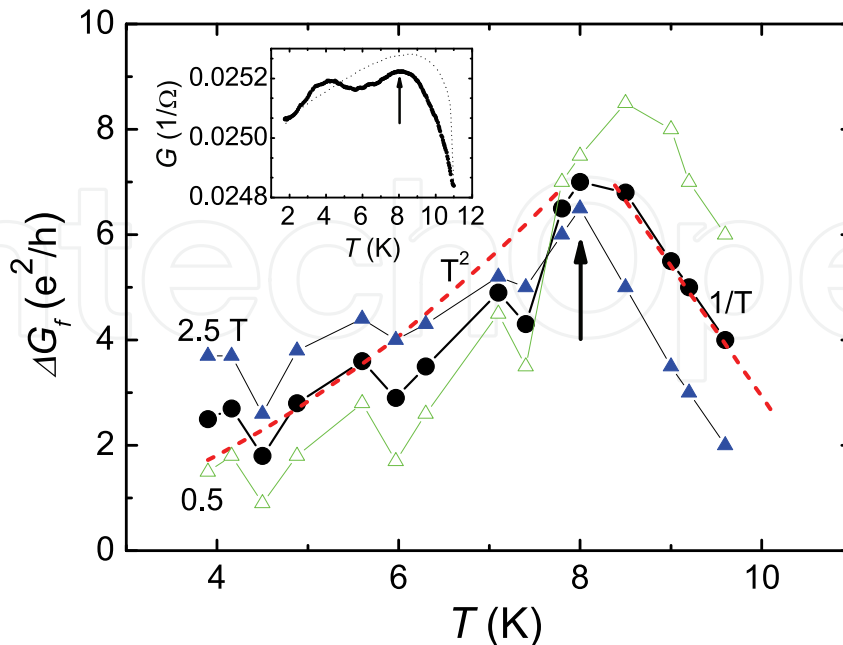


Fig. 13. Fluctuation amplitude as a function of temperature. Two curves for different magnetic field regime are shown in 0.5 (open triangles) and 2.5 T (filled triangles), and the average of the two curves is shown by filled circles. The dashed curve shows the T^2 behavior at $T < 8$ K and the $1/T$ behavior at $T > 8$ K in theory. Inset: the temperature dependence of conductance (filled circle curve) and calculated conductance (thin dashed curve)

experiments on metal and 2DEG semiconductor (den Hartog et al.,1996; Akazaki et al.,2004). The higher E_{th} was observed in our experiment because of high D . We estimated the diffusion constant D of network-like CNTs by $D = v_F l_e$, where v_F is the Fermi velocity about 8×10^5 m/s (Lee et al.,2004), and l_e is the mean free path. Because pure CNT has the property of ballistic transport, the length between crossed junctions corresponds to l_e . The l_e of ~ 0.15 μm was obtained by counting the crossed junction number of CNT, about 11~4, between electrodes as shown in Fig. 2 (bottom figure). Thus, D is calculated to be about $0.07 \sim 0.18$ m^2/s , which is larger than the previous experiment value by 1~2 orders of magnitude. Using averaged value $D = 0.12$ m^2/s , we calculated the conductance as a function of temperature (dash curve) by the Usadel equation to compare it to our experimental result in the inset of Fig. 13 (see (Akazaki et al.,2004) for detail). The variation in conductance due to the proximity effect is defined as $\Delta G_{N'} = (G_N - G_{N0})/G_{N0}$, where G_N is the conductance of the SN junction measured at zero-bias voltage and G_{N0} is that measured at high temperature, where the proximity effect can be neglected. The details of the function $\Delta G_{N'}$ are given by Golubov et. al (Golubov,Wilhelm&Zaikin,1997). The result of calculation is $G = A \times \Delta G_{N'} \times G_{N0} + G_{N0}$, where free parameter A is 0.165 and G_{N0} is 24.84 mS [the inset of Fig. 13]. The temperature of maximum conductance in the theoretical prediction, $T_m (\sim E_{th}/k_B)$, $\simeq 9$ K, which is very close to the measured value of 8 K.

The fluctuation amplitude is estimated by evaluating the bandwidth in a range of magnetic field such as at 8 K (inset of Fig. 10). Fig. 13 shows three curves of $\Delta G_f(T)$ between 10 to 4 K. The evaluated $\Delta G_f(T)$ at applied magnetic field around 0.5 (open triangles) and 2.5 T (closed triangles) are shown. The averaged $\Delta G_f(T)$ (closed circle)

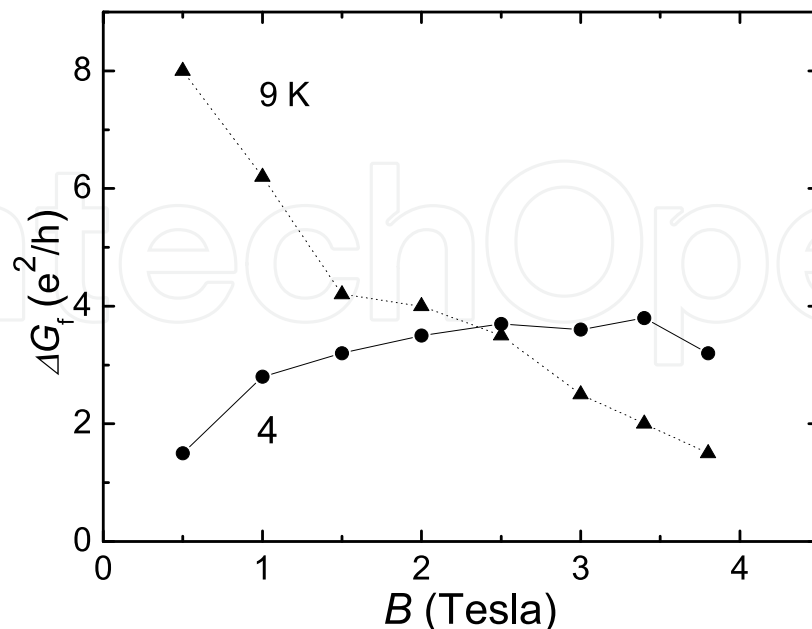


Fig. 14. Fluctuation amplitude as a function of magnetic field. Two curves for different temperature are shown by filled circle (4 K) and filled triangles (9 K)

from the curves of 0.5 and 2.5 T is also shown in between two curves. This averaged $\Delta G_f(T)$ becomes small as low temperature is approached and reaches a maximum amplitude at 8 K, which is related to E_{th} , and this T_m of 8 K is the same as the T_m of conductance in the insert of Fig. 13. Theoretically, the model has been constructed by the proximity correction to quasi-1D normal conductor with the loop of AB-type oscillation and the reentrant behavior of $\Delta G_f(T)$ has been predicted (Golubov, Wilhelm & Zaikin, 1997; Nakano & Takayanagi, 2000). When $T > T_m$, $\Delta G_f(T)$ is proportional to $1/T$. This can be explained by a simple physical interpretation: Superconductivity penetrates a distance with temperature between the two electrodes, whereas the rest keeps normal conductivity and, because the distance of the rest is proportional to T , the resistance of the rest is proportional to T (Golubov, Wilhelm & Zaikin, 1997). This means that the enhanced $\Delta G_f(T)$ is proportional to $1/T$. The electron coherent length should be shorter than the electrode spacing and the MTSF effect dominates the behavior of $\Delta G_f(T)$. In the limit $T < T_m$, the electron coherent length is longer than the electrode spacing and the DDOS effect is enhanced, and then $\Delta G_f(T)$ exhibits a diminishment behavior of T^2 as T approaches 0. Experimentally, for enhanced $\Delta G_f(T)$ behavior had only been observed, but diminishment behavior has never been observed, to the best of our knowledge. As shown in Fig. 13, the reentrant behavior of $\Delta G_f(T)$ are observed in $T < 8$ K regimes, and the dashed curve was predicted in theory.

We also investigated the ΔG_f with the magnetic field in the case of two limits. The behavior of $\Delta G_f(B)$ is shown at 9 K ($> T_m$) in Fig. 14. The $\Delta G_f(B)$ is reduced with increasing magnetic field and exhibits a monotonic behavior. This behavior due to the MTSF effect is smeared by increasing the magnetic field gradually. At 4 K ($< T_m$), the $\Delta G_f(B)$ with an applied magnetic field exhibits a nonmonotonic behavior (Fig. 14), because this behavior is a reentrant behavior. Both DDOS effect and the MTSF effect have the same

contribution in $\Delta G_f(T)$ behavior as T approaches 0, but the DDOS effect is more sensitive to the magnetic field than the MTSF effect. According to the quasiparticles transport process in Nakano's theory (Nakano&Takayanagi,2000), DDOS effect needs time reversal symmetry that is twice as long as that needed by the MTSF effect. Therefore, the DDOS effect should be more sensitive and be smeared more heavily than the MTSF effect. The conductance diminishment (DDOS effect) of the rapid decay with the increase of the energies (T or V) occurs for the same reason and the reentrant behavior on T or V has also been observed in nonmonotonic $\Delta G_f(B)$ behavior. The $\Delta G_f(B)$ becomes small with increasing strength of the field and reaches a maximum amplitude at 2.5 ~ 3.5 T as correlation magnetic field B_c , which is related to E_{th} . This nonmonotonic behavior can also be seen in the differential resistance of zero-bias voltage with magnetic field in Fig. 6 that shows changes from a peak to a dip and then back to a peak again. The B_c can be estimated by $B_c \sim \Phi_0/L_\phi^2$, where Φ_0 is $h/2e$, because the magnetic field required to destroy the interferences can be determined by one flux quantum through the area of the largest possible phase coherent path (Dikin et al.,2001). For AR in a CNT, an electron is incident into the interface and should be Andreev reflected into the same CNT. Since the AR process is phase coherent, the retroreflected hole can interfere with incident electron. The quasiparticles are induced by localized AR, but are not affected by the network structures of the CNTs. We can obtain $B_c = 3.3$ T by $B_c \sim h/2eLW$ (Washburn&Webb,1992; Dikin et al.,2001), where the width of the wire $W = 1$ nm and the length $L = 1 \mu\text{m}$ are the carbon nanotube diameter and electrode spacing. The B_c is much higher than in previous experiments with only a few microtesla in metallic wires (Dikin et al.,2001). Because this high B_c , the reentrant behavior of $\Delta G_f(B)$ can be observed. Here, we emphasize that this result is difficult to be observed in normal metals or 2DEG semiconductor, because the enhanced $\Delta G_f(B)$ could not be easily observed in previous experiments with only low B_c . There is a unique characteristic in network-like ultra-thin CNTs. The high B_c is due to the ultra-thin tubes and fluctuation oscillation is due to the network-like structures.

6. The theoretical analysis of enhanced quantum interference and reentrant behavior for network structure

Since the total conductance of the junction is the conductance of the series of the interface G_T and the diffusive G_N part such that

$$G = \frac{1}{1/G_T + 1/G_N},$$

the conductance change is approximately given by

$$\Delta G \simeq \frac{G_{N0}^2 \Delta G_T + G_{T0}^2 \Delta G_N}{(G_{N0} + G_{T0})^2},$$

where $G_N = G_{N0} + \Delta G_N$, $G_T = G_{T0} + \Delta G_T$.

In this expression, only ΔG_N shows so-called "re-entrant behavior" as a function of applied voltage V , temperature T , or applied magnetic field B . ΔG_T is not so sensitive to the applied field, voltage, or temperature, when the measurement temperature is sufficiently lower than the bulk superconducting gap Δ ; $V, T \ll \Delta$, and when the applied field is much smaller than

the critical one; $B \ll B_c$. Therefore, we make ΔG_T a constant. Then,

$$\Delta G(V, T, B) = \frac{G_{N0}^2 \Delta G_T + G_{T0}^2 \Delta G_N(V, T, B)}{(G_{N0} + G_{T0})^2},$$

and, we can thusly discuss the conductance change as the functions of T, B, V :

$$\delta G(V, T, B) = K_0 \Delta G_N(V, T, B),$$

with a constant

$$K_0 = \frac{G_{T0}}{(G_{N0} + G_{T0})^2}.$$

The proximity correction to this conductance $\Delta G_N(V, T, B)$ disappears at low energies and reaches a maximum value around temperature T or bias voltage V corresponding to the Thouless energy (correlation energy). In a quasi 1D quantum wire, the correlation magnetic field for breaking the time reversal symmetry (electron-hole symmetry) is given by $B_c \sim h/2eLW$. On the other hand, correlation energy for the Maki-Thompson enhancement and the decreased quasiparticle density of states effect effect is the Thouless energy $E_{Th} = \hbar D/L^2$. Therefore, the reentrant behavior in ΔG_N happens near $eV = E_{Th}$, $k_B T = E_{Th}$, or $B = B_c$.

Let us consider an AB-type interferometer formed by quasi 1D wires and placed between the S and N electrodes. The AB oscillation amplitude in ΔG_N is the order of G_{T0}^2/G_{N0} , and it should change as a function of T, V in the same way it does in a single quasi 1D wire. The explicit form of $\Delta G_N(V, T, B)$ as the function of V, T, B has been given in many literatures (Golubov, Wilhelm & Zaikin, 1997; Volkov & Takayanagi, 1997; Nakano & Takayanagi, 2000). Here, we drop the expression for an AB ring in Nakano and Takayanagi's eq. (51) (Nakano & Takayanagi, 2000) because it is convenient for our present purpose. Thus, we have

$$\begin{aligned} \delta G(\Psi = 0) - \delta G(\Psi) &\sim \frac{K_0 G_T^2 E_{Th}}{G_{N0} k_B T} \exp \left[-\frac{\pi R_0}{\pi R_0 + L_L} \right] \\ &\simeq \frac{G_{T0}^4}{G_{N0} (G_{T0} + G_{N0})^2} \frac{E_{Th}}{k_B T} \exp \left[-\frac{\pi R_0}{\pi R_0 + L_L} \right] \end{aligned} \quad (1)$$

where R_0 is the radius of the ring and $L_L = L - \pi R_0$ is the length of the wire except for the loop part (that is, the length of the lead). When the tunnelling conductance is much smaller than the diffusive part, i.e. $G_{T0} \ll G_{N0}$, the original expression is recovered. In contrast, when G_{T0} is comparable to G_{N0} , the amplitude of the fluctuation is large.

The oscillation period is Ψ_0 with the flux piercing the AB ring, where Ψ_0 is the flux quantum. It should be noted that the period is half that of a usual AB oscillation because this is an interference of the proximity-induced quasiparticle.

The experimental results show that the amplitude of the oscillation is for times e^2/h or larger and that the dominant characteristic period is approximately 500 Gauss (See Fig. 10). From the period, we estimate the radius of the dominant loop structure to be about 150 nm. It is postulated that there are many loop structures in the CNT region. Since the distance between the S and N electrode is 1 μm , can be neglected, the exp factor in eq. (1)

In order to analyze the amplitude of the fluctuation, we need a model of the CNT region. Suppose that the CNT region is a random network formed by many CNTs. For simplicity, let us assume a irregular lattice of CNTs. There are n CNTs bridging the S and N electrodes. We

call them longitudinal CNTs. In the direction perpendicular to the bridge CNTs, m CNTs are distributed, and we call them transverse CNTs. At the first step, we neglect the conductance of the barrier contacting a longitudinal CNT and transverse. The average conductance of the CNT region is the same as that of n times of a single CNT. A single CNT has a conductance of the order of e^2/h or less. Experimentally, the value of the total conductance is about $650e^2/h$; therefore, $n > 650$.

The lattice network has many loops with different areas. We assume that the dominant radius is what we estimated above. Therefore, the period of the oscillation in each loop is almost the same. However, the phase of the oscillation is different in each loop. Then, the oscillation amplitude in the total conductance is enhanced by the factor \sqrt{s} , where s is the number of loops with almost the same dominant radius in the lattice. The \sqrt{s} dependence comes as follows. The conductance oscillations of loops are superposed. However, the effect of distributed oscillation causes an averaging effect. So, s/\sqrt{s} gives \sqrt{s} .

When we put the conductance of a single CNT as $G_{N0} = \alpha e^2/h$ and the conductance across the S electrode and a single CNT as $G_{T0} = \beta G_{N0}$, the expected amplitude of the oscillation is

$$\sqrt{s} \frac{G_{T0}^4}{G_{N0}(G_{T0} + G_{N0})^2} \frac{E_{Th}}{k_B T} \simeq \frac{\sqrt{s} \alpha \beta^4}{(1 + \beta)^2} \frac{e^2}{h}$$

when $k_B T = E_{th}$. On the other hand,

$$n \times \frac{1}{\frac{1}{\alpha e^2/h} + \frac{1}{\beta \alpha e^2/h}} \simeq 650e^2/h \quad (2)$$

should be satisfied because this corresponds to the total conductance of the SN junction. When we take into account the barrier conductance across the longitudinal and transverse CNT contact, the amplitude is reduced. We put the factor as z . From the observed oscillation amplitude $4e^2/h$, we have

$$z \frac{\sqrt{s} \alpha \beta^4}{(1 + \beta)^2} \simeq 4. \quad (3)$$

For example, $n = 2000$, $\alpha = 0.9$, $\beta = 0.56$, $s = 1.8 \times 10^6$ and $z = 0.5$ satisfies both (2) and (3). The number of the loops, s , is very large; however, it is not impossible when the number of the transverse CNTs, m , is more than 1000.

The conductance of the diffusive region G_{N0} is much bigger than that of the interface G_{T0} . For example, we put $G_{T0} = 0.01G_{N0}$. The measured conductance of the junction, $\sim 650e^2/h$, is mainly determined by G_{T0} because the interface and the diffusive wire are serially connected. Then, we can put $G_{T0} \sim 650e^2/h$ and $G_{N0} \sim 65000e^2/h$. However, the amplitude $\sim 4e^2/h$ is smaller than the expected one:

$$\frac{G_{T0}^4}{G_{N0}(G_{T0} + G_{N0})^2}$$

with $k_B T = E_{Th}$. When we use $G_{T0} = 0.01G_{N0}$, and $G_{N0} = 65000e^2/h$, the expected fluctuation is about $6e^2/h$.

7. Conclusion

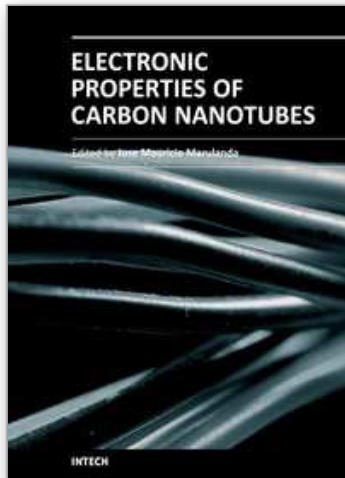
The multiple Andreev reflection and the enhanced magnetoconductance fluctuations, such as an superconducting UCFs, were observed in S/network-like CNTs/S junctions. The reentrant behavior was observed and consisted with each other in the temperature and voltage

dependence of conductance, and in the dependence of fluctuation amplitude on temperature and magnetic field. Especially, the reentrant behavior of $\Delta G_f(T)$ was first observed as diminished $\Delta G_f(T) \sim T^2$ as T approached 0 and the reentrant behavior of $\Delta G_f(B)$ was also observed. We found that the high critical magnetic field destroys Andreev reflection process and the high correlation magnetic field induces the dephasing of interference in CNTs, which are larger than that for 2D SNS junctions by about two orders of magnitude. These results are due to the small diameter of the CNTs with network-like structures.

8. References

- [Akazaki et al., 2004] Akazaki, T., Yamaguchi, H. and Takayanagi, H. (2004). Nonequilibrium-GaAs(111) a heterostructures coupled with superconducting Nb electrodes. *Semicond. Sci. Technol.* Vol. 19 (2004)S182-S184.
- [Bezuglyi et al., 2000] Bezuglyi, E. V., Bratus, E. N., Shumeiko, V. S., Wendin G. and Takayanagi, H. (2000). Circuit theory of multiple Andreev reflections in diffusive SNS junctions. *Phys. Rev. B* Vol. 62, No. 21 (December 2000) 14439-14451.
- [Bockrath et al., 1999] Bockrath, M., et al. (1999). Luttinger-liquid behaviour in carbon nanotubes. *Nature* Vol. 397, (18 February 1999), 598-601.
- [Buitelaar et al., 2003] Buitelaar, M. R., Belzig, W., Nussbaumer, T., Babic, B., Bruder, C. and Schonberger, C. (2003). Multiple Andreev Reflections in a Carbon Nanotube Quantum Dot. *Phys. Rev. Lett.* Vol. 91, No. 5 (2003) 57005-1 - 57005-4.
- [Cleuziou et al., 2006] Cleuziou, J. -P. (2006). Carbon nanotube superconducting quantum interference device. *Nature Nanotech.* Vol. 1 (October 2006)53-59.
- [den Hartog et al., 1996] den Hartog, S. G., Kateyn, C. M. A., van Wees, B. J., Klapwijk, T. M., van der Graaf, W. and Borghs, G. (1996). Sample-Specific Conductance Fluctuations Modulated by the Superconducting Phase. *Phys. Rev. Lett.* Vol. 76, No. 24, (1996)4592-4595; Charlat, P., Courtois, H., Gandit, Ph., Mailly, D., Volkov, A. F., and Pannertier, B. (1996). *Phys. Rev. Lett.* Vol. 77, No. 24, (1996)4950-4953; Chien, C. -J. and Chandrasekhar, V. (1999). Reentrance effect in normal-metal/superconducting hybrid loops. *Phys. Rev. B* Vol. 60, No. 22, (1999)15356-15363.
- [Dirks et al., 2011] Dirks, Travis, Hughes, Taylor L., Lal, Siddhartha, Uchoa, Bruno, Chen, Yung-Fu, Chialvo, Cesar, Goldbart, Paul M. and Mason, Nadya. (2011). Transport through Andreev bound states in a graphene quantum dot. *Nature Physics* (6 February 2011)1-5; Du, Xu, Skachko, Ivan and Andrei, Eva Y. (2008). Josephson current and multiple Andreev reflections in graphene SNS junctions. *Phys. Rev. B* Vol. 77, (2008)184507-1-184507-5; Heersche, Hubert B., Jarillo-Herrero, Pablo, Oostinga, Jeroen B., Vandersypen, Lieven M. K., and Morpurgo, Alberto F. (2007). Bipolar supercurrent in graphene. *Nature*, Vol. 446, (1 March 2007)56-59.
- [Dikin et al., 2001] Dikin, D. A., Black, M. J., and Chandrasekhar, V., (2001). Magnetoresistance of Proximity-Coupled Au Wires. *Phys. Rev. Lett.* Vol. 87, No. 18, (2001)187003-1-187003-4.
- [Golubov, Wilhelm & Zaikin, 1997] Golubov, A. A., Wilhelm, F. K., and Zaikin, A. D. (1997). Coherent charge transport in metallic proximity structures. *Phys. Rev. B* Vol. 55, No. 2, (1997)1123-1137.

- [Hoss et al., 2000] Hoss, T., Strunk, C., Nussbaumer, T., Huber, R., Staufer, U. and Schonenberger, C. (2000). Multiple Andreev reflection and giant excess noise in diffusive superconductor normal-metal superconductor junctions. *Phys. Rev. B* Vol. 62, No. 6 (2000) 4079-4085.
- [Jarillo-Herrero et al., 2006] Jarillo-Herrero, Pablo, Dam, Jordan A. van and Kouwenhoven, Leo P. (2006). Quantum supercurrent transistors in carbon nanotubes. *Nature* Vol. 439, (23 February 2006) 953-956.
- [Jorgensen et al., 2006] Jorgensen, H. I., et al. (2006). Electron Transport in Single-Wall Carbon Nanotube Weak Links in the Fabry-Perot Regime. *Phys. Rev. Lett.* Vol. 96, (2006) 2070031-1-2070031-4.
- [Kasumov et al., 1999] Kasumov, A. Yu., Deblock, R., Kociak, M., Reulet, B., Bouchiat, H., Khodos, I. I., Gorbatov, Yu. B., Volkov, V. T., Journet, C., and Burghard, M. (1999). Supercurrents Through Single-Walled Carbon Nanotubes. *Science* Vol. 284, (28 May 1999) 1508-1510.
- [Lee et al., 2004] Lee, Jinhwan, Eggert, S., Kim, H., Kahng, S. -J. Shinohara, H., and Kuk, Y. (2004). Real Space Imaging of One-Dimensional Standing Waves Direct Evidence for a Luttinger Liquid. *Phys. Rev. Lett.* Vol. 93, No. 16, (2004) 1664031-1-1664031-4.
- [Morpurgo et al., 1999] Morpurgo, A. F., Kong, J., Marcus, C. M. and Dai, H. (1999). Gate-Controlled Superconducting Proximity Effect in Carbon. *Science* Vol. 286 (8 October 1999) 263-265.
- [Mortensen et al., 1999] Mortensen, N. A., Flensberg, K., and Jauho, A. P. (1999). Angle dependence of Andreev scattering at semiconductor-superconductor interfaces. *Phys. Rev.* Vol. 59, No. 15, (1999) 10176-10182.
- [Nakano & Takayanagi, 2000] Nakano, H., and Takayanagi, H. (2000). Influence of phase quantum fluctuations on superconducting proximity correction in normal-metal wire conductance. *Phys. Rev. B* Vol. 61, No. 22, (2000) 15398.
- [Nitta et al., 1994] Nitta, J., Akazaki, T. and Takayanagi, H. (1994). Magnetic-field dependence of Andreev reflection in a clean Nb-InAs-Nb junction. *Phys. Rev. B* Vol. 49, No. 5 (1994) 3659-3662.
- [Octavio et al., 1983] Octavio, M., Tinkham, M., Blonder, G. E. and Klapwijk, T. M. (1983). Subharmonic energy-gap structure in superconducting constrictions. *Phys. Rev. B* Vol. 27, No. 11 (1983) 6739-6746.
- [Pillet et al., 2010] Pillet, J.-D., Quay, C. H. L., Morfin, P., Bena, C., Levy Yeyati, A. and Joyez, P. (2010). Andreev bound states in supercurrent-carrying carbon nanotubes revealed. *Nature Physics* Vol. 6, 965-969 (2010).
- [Rao et al., 1997] Rao, A. M., Richter, E., Bandow, S., Chase, B., Eklund, P. C., Williams, K. A., Fang, S., Subbaswamy, K. R., Menon, M., Thess, A., Smalley, R. E., Dresselhaus, G., and Dresselhaus, M. S. (1997). Diameter-Selective Raman Scattering from Vibrational Modes in Carbon Nanotubes. *Science* Vol. 275 (1997) 187-191.
- [Volkov & Takayanagi, 1997] Volkov, A. F., and Takayanagi, H. (1997). Long-range phase-coherent effects in the transport properties of mesoscopic superconductor-normal-metal structures. *Phys. Rev. B* Vol. 56, (1997) 11184.
- [Washburn & Webb, 1992] Washburn S., and Webb, R. A. (1992). Quantum transport in small disordered samples from the diffusive to the ballistic. *Rep. Prog. Phys.* Vol. 55, (1992) 1311.



Electronic Properties of Carbon Nanotubes

Edited by Prof. Jose Mauricio Marulanda

ISBN 978-953-307-499-3

Hard cover, 680 pages

Publisher InTech

Published online 27, July, 2011

Published in print edition July, 2011

Carbon nanotubes (CNTs), discovered in 1991, have been a subject of intensive research for a wide range of applications. These one-dimensional (1D) graphene sheets rolled into a tubular form have been the target of many researchers around the world. This book concentrates on the semiconductor physics of carbon nanotubes, it brings unique insight into the phenomena encountered in the electronic structure when operating with carbon nanotubes. This book also presents to reader useful information on the fabrication and applications of these outstanding materials. The main objective of this book is to give in-depth understanding of the physics and electronic structure of carbon nanotubes. Readers of this book should have a strong background on physical electronics and semiconductor device physics. This book first discusses fabrication techniques followed by an analysis on the physical properties of carbon nanotubes, including density of states and electronic structures. Ultimately, the book pursues a significant amount of work in the industry applications of carbon nanotubes.

How to reference

In order to correctly reference this scholarly work, feel free to copy and paste the following:

Yuan-Liang Zhong, Hayato Nakano, Tatsushi Akazaki and Hideaki Takayanagi (2011). Multiple Andreev Reflection and Enhanced Quantum Interferences in NbN/Network-Like Carbon Nanotubes/NbN SNS Junctions, *Electronic Properties of Carbon Nanotubes*, Prof. Jose Mauricio Marulanda (Ed.), ISBN: 978-953-307-499-3, InTech, Available from: <http://www.intechopen.com/books/electronic-properties-of-carbon-nanotubes/multiple-andreev-reflection-and-enhanced-quantum-interferences-in-nbn-network-like-carbon-nanotubes->

INTECH
open science | open minds

InTech Europe

University Campus STeP Ri
Slavka Krautzeka 83/A
51000 Rijeka, Croatia
Phone: +385 (51) 770 447
Fax: +385 (51) 686 166
www.intechopen.com

InTech China

Unit 405, Office Block, Hotel Equatorial Shanghai
No.65, Yan An Road (West), Shanghai, 200040, China
中国上海市延安西路65号上海国际贵都大饭店办公楼405单元
Phone: +86-21-62489820
Fax: +86-21-62489821

© 2011 The Author(s). Licensee IntechOpen. This chapter is distributed under the terms of the [Creative Commons Attribution-NonCommercial-ShareAlike-3.0 License](#), which permits use, distribution and reproduction for non-commercial purposes, provided the original is properly cited and derivative works building on this content are distributed under the same license.

IntechOpen

IntechOpen